Homeostatic maintenance of non-structural carbohydrates during the 2015-2016 El Niño drought across a tropical forest precipitation gradient

Running title: homeostasis of tropical forest carbohydrates

L. Turin Dickman[1*], Nate G. McDowell[2], Charlotte Grossiord[3], Adam D. Collins[1], Brett T. Wolfe[4], Matteo Detto[5], S. Joseph Wright[4], José A. Medina-Vega[4,6], Devin Goodsman[1], Alistair Rogers[7], Shawn P. Serbin[7], Jin Wu[7], Kim S. Ely[7], Sean T. Michaletz[8], Chonggang Xu[1], Lara Kueppers[9], and Jeffrey Q. Chambers[9]

[1]Earth & Environmental Sciences Division, Los Alamos National Laboratory, Los Alamos, NM 87545, USA

[2] Earth Systems Analysis & Modeling, Pacific Northwest National Laboratory, Richland, WA 99352, USA

[3]Swiss Federal Research Institute WSL, 8903 Birmensdorf, Switzerland

[4]Smithsonian Tropical Research Institute, Apartado 0843-03092, Balboa, Panama

[5]Ecology and Evolutionary Biology Department, Princeton University, Princeton, NJ 08540, USA

[6]Forest Ecology and Forest Management Group, Wageningen University and Research, PO Box 47, 6700 AA Wageningen, The Netherlands

[7]Environmental & Climate Sciences Department, Brookhaven National Laboratory, Upton, New York, NY 11973, USA

[8]Department of Botany and Biodiversity Research Centre, University of British Columbia, Vancouver, BC V6T 1Z4, Canada

[9]Earth and Environmental Sciences Area, Lawrence Berkeley National Laboratory, Berkeley, CA 94720, USA

*Corresponding author: L. Turin Dickman, +1 (505) 665-4437, lee@lanl.gov

Proposed journal: Plant, Cell and Environment

Abstract: Non-structural carbohydrates (NSCs) are essential for maintenance of plant metabolism, and may be sensitive to both short- and long-term climatic variation. NSC variation in moist tropical forests has rarely been studied, so regulation of NSCs in these systems is poorly understood. We measured foliar and branch NSC content in 23 tree species at three sites located across a large precipitation gradient in Panama during the 2015-2016 El Niño to examine how short- and long-term climatic variation impact carbohydrate dynamics. Across all sites, leaf NSCs increased over diurnal time-periods. There was no significant difference in total NSCs as the drought progressed (leaf $p=0.32$, branch $p=0.30$), nor across the rainfall gradient (leaf $p=0.91$, branch $p=0.96$). Foliar soluble sugars decreased while starch increased over the duration of the dry period, suggesting greater partitioning of NSCs to storage than metabolism or transport as drought progressed. There was large variation across species at all sites, but total foliar NSCs were positively correlated with leaf mass per area, while branch sugars were positively related to leaf temperature and negatively correlated with daily photosynthesis and wood density. The NSC homeostasis across a wide range of conditions suggests that NSCs are an allocation priority in moist tropical forests.

Keyword index: NSC; Panama; ENSO; tropics; climate; storage; sugars; vegetation

Introduction

Tropical forests account for a large fraction of terrestrial live biomass (Pan et al., 2013) and approximately half of terrestrial gross primary production (GPP; Beer et al., 2010). Drought is one of the largest threats to tropical forest structure and functioning (Davidson et al. 2012; McDowell et al. 2018), and can result in reduced carbon sequestration due to higher ecosystem respiration and lower GPP (Cavaleri et al. 2017), transitioning these ecosystems from carbon sinks to sources (Tian et al. 1998). The El Niño phase of the El Niño Southern Oscillation (ENSO) impacts some tropical forests through hotter, drier dry seasons and wet seasons with less solar insolation (Cavaleri et al. 2017). El Niños occur sub-decadally (Allan et al. 1996), and extreme events are expected to increase in frequency with climate change (Cai et al. 2014). Droughts with and without El Niños have been associated with increased mortality of canopy trees (Condit et al. 1996, Laurance & Williamson 2001), as well as shifts in allocation from leafing to fruiting (Laurance & Williamson 2001, Detto et al. 2018), and altered remote sensing signatures of the canopy surface (e.g. greenness, backscatter; Li et al. 2018, Nagai, Ichii, & Morimoto. 2007; Saatchi et al. 2013).

Non-structural carbohydrates (NSCs) provide the carbon skeletons for biosynthetic pathways associated with secondary metabolism (e.g. growth and defense), and for energy production (i.e. respiration through glycolysis and the tricarboxylic acid cycle; Chapin et al. 1990, Heldt 2005). Constraints on NSC storage and utilization have prompted widespread research on their role in autotrophic carbon cycling (e.g. Dietze et al. 2014) and in the avoidance of carbon starvation (e.g. Adams et al. 2017). NSCs are stored, typically as starch, when supply of photosynthate exceeds demand (i.e. when carbon assimilation is greater than growth and metabolism; McDowell 2011). These stored NSCs can then be utilized during periods when

supply is unable to match demand (e.g. during periods when CO_2 assimilation may be reduced; Hoch et al. 2003). Furthermore, deep reserves of NSCs older than one decade may even be utilized in growth and respiration, thus providing some buffer to seasonal variation (Dietze et al. 2014, Martinez-Vilalta et al. 2016).

In a global review of NSC dynamics across organs, Martinez-Vilalta et al. (2016) found that seasonal minimums remained relatively high and constant among functional types and biomes, supporting the idea that NSCs are maintained above some (undetermined) minimum threshold. They also found that, while depletion of starch was relatively common, depletion of soluble sugars or total NSCs was very rare, consistent with the role of starch as a storage reservoir and soluble sugars as substrate for immediate metabolic use. Relative to other biomes, tropical systems showed low seasonal variability in NSCs (Martinez-Vilalta et al. 2016).

Data from the tropics, however, remains relatively limited. Less than 15% of studies in the global review by Martinez-Vilalta et al. (2016) were from the tropics, and several of these were performed on seedlings or understory shrubs. Several studies have shown a positive relationship between NSCs and tropical seedling survival during periods of stress (Newell et al. 2002, Meyers & Kitajima 2007, Poorter & Kitajima 2007, Poorter et al. 2010, O'Brien et al. 2014), as well as higher seedling NSC concentrations in species from wetter tropical forests (Poorter & Kitajima 2007). An accumulation of NSCs prior to or during seasonal drought is commonly observed (Würth et al. 1998, Latt et al. 2001, Newell et al. 2002, Körner 2003, Würth et al. 2005), particularly for deciduous trees (Newell et al. 2002), but this rise is small in comparison to the extra-tropical biomes (Martinez-Vilalta et al. 2016). This is consistent with the observed increase in NSCs associated with lower growth rates in stressed seedlings (Meyers & Kitajima 2007, Poorter & Kitajima 2007, Poorter et al. 2010) and suggests storage accumulation

as growth slows. Results from a long-term precipitation throughfall reduction experiment on mature trees showed no difference in NSCs between surviving droughted and control trees (Rowland et al. 2015), suggesting that at longer time periods during which mortality (thinning) occurs, NSCs may also be homeostatically regulated, in part by stand-scale processes (e.g. McDowell et al. 2006).

These studies, along with recent evidence from the temperate zone (Schoenbeck et al. 2018), suggest that NSCs may increase, even if only slightly, in response to seasonal drought in tropical forests. However, across sites, acclimation of leaf and plant traits such as height, leaf area, leaf mass per area, and stand density, may allow homeostatic mainentence of NSC concentrations; that is, they maintain relatively stable values despite long-term environmental variation (see for example homeostasis of NSCs e.g. Rowland et al. 2015; leaf gas exchange e.g. Ehleringer and Cerling 1995, McDowell et al. 2006; or temperature e.g. Michaletz et al. 2015, 2016, Blonder and Michaletz 2018). The 2016 El Niño presented a unique opportunity to test the hypotheses that seasonal shifts will occur during drought within sites, and that adaptation may allow homeostatic maintenance of NSCs across a long-term rainfall gradient. No prior study of NSCs in tropical forests has considered multiple sites and multiple dates throughout a seasonal drought, allowing investigation into short-term drought response (within sites) simultaneous with long-term acclimation response (across the precipitation gradient). We collected canopy tree NSCs across the Isthmus of Panama for the duration of the 2016 dry period,within the 2015-2016 El Niño period. We expected mild to moderate dry-season increases in NSCs (Würth et al. 1998, Latt et al. 2001, Körner 2003, Würth et al. 2005) with homeostatic maintenance of NSCs across sites despite widely differing climatic regimes (Table 1). We hypothesized that NSCs would

instead vary with intrinsic physiological traits (e.g. photosynthesis, leaf and hydraulic traits) that can be mechanistically related to NSC dynamics.

Materials and Methods

Site descriptions

We used three lowland tropical forest sites located across a precipitation gradient on the Isthmus of Panama for this study. Two of the sites have canopy-access cranes, maintained by the Smithsonian Tropical Research Institute, enabling sampling and measurement at the top of the forest canopy. The two canopy-access sites include a seasonally dry forest in the Parque Natural Metropolitano (PNM) near Panama City and a wet evergreen forest in the San Lorenzo Protected Area (SLZ), Colon Province. The third, and intermediate, site is located on Barro Colorado Island (BCI) in the Panama Canal. Historic (1998-2015) mean annual air temperature (± standard deviation) is 26.0 (± 0.6) °C, 25.9 (± 0.7) °C, and 25.3 (± 0.6) °C, and mean annual precipitation is 1844 mm, 2352 mm, and 3282 mm for PNM, BCI, and SLZ, respectively, with ~85% of rainfall in the May-November wet season (Fig. 1, Table 1; data provided by the Physical Monitoring Program of the Smithsonian Tropical Research Institute.). For more site information, refer to Basset et al. (2003).

Twenty-three locally abundant canopy tree species (PNM n=9; BCI n=5; SLZ n=9) were selected for intensive measurement of leaf NSCs and other traits (see Tables S1,S2, and S3 for more information). Four monthly campaigns were conducted over the course of the 2016 dry season from mid-February to mid-May (Fig. 1). During each campaign, two days were spent at each location (except BCI; see below) conducting diurnal measurements of leaf gas exchange and traits (see Table S1) on fully-expanded, upper canopy sunlit foliage of one target tree of each

species. Target species were selected to cover a wide range of wood densities. Individuals with low or no liana infestation were chosen based on crane or tower access (see below). The same individuals ("target trees") were sampled during each campaign (see Table S3 for target tree attributes). At PNM and SLZ leaves were measured and sampled via canopy-access cranes. At BCI leaves were sampled from two telecommunication towers or by sling-shot, precluding measurement of *in-situ* leaf gas exchange and branch sampling for NSC analysis and A-C_i curves. BCI was only sampled in March due to the logistical difficulty of accessing the upper canopy. Branches were sampled at PNM in March and at SLZ in March and April (see Table S4 for NSC sampling schematic) as described below.

Leaf gas exchange and ecophysiological traits

Leaf gas exchange and temperature were measured with 5-6 portable gas exchange systems (LI-6400XT, LI-COR Inc., Lincoln, NE, USA) equipped with 2x3 cm^2 leaf chambers and red-blue light sources, and zeroed with a common nitrogen standard prior to each campaign. Diurnal leaf gas exchange measurements (dataset available online, Rogers et al. 2017a) were made on two to three leaves of each target tree using the canopy-access cranes at PNM and SLZ as described previously (Rogers et al. 2004). Measurements were conducted approximately every two to three hours from 6:00 to 19:00 local time for a total of five to seven measurements per day. Chamber conditions mimicked outdoor conditions of humidity, temperature, and photosynthetically active radiation. Leaf temperature was measured by a thermocouple in the chamber during gas exchange measurement. Following *in-situ* gas exchange measurements, leaves were immediately harvested for trait measurements. Leaves were sealed in humidified plastic bags and stored in the dark, on ice for a maximum of 2 hours before further processing.

Leaf water potential (Ψ_l, MPa; dataset available online, Wolfe et al. 2017) was measured using a pressure chamber (PMS, Albany, OR, USA). Following measurement, a known leaf area was sampled with cork borers, weighed with a precision balance (Fisher Science Education, Model SLF303, Hanover Park, IL), then dried to constant mass at 70°C for determination of dry mass and calculation of leaf mass per area (LMA, g m^{-2}; dataset available online, Ely et al. 2017). Additional leaf punches were collected for NSC analysis at early (first after pre-dawn, ~6:00-9:00), mid-day (between ~11:30-14:30), and late (last before sun-down, ~16:00-19:00) diurnal time points and treated as described below (see *Non-structural Carbohydrate Analysis*). Leaf samples were also collected before dawn to measure pre-dawn leaf water potential (Ψ_{PD}, MPa).

First-order branches at PNM and SLZ were collected at pre-dawn and kept in the shade for measurement of A-C_i curves (dataset available online, Rogers et al. 2017b). Immediately after harvesting, branches were re-cut under water, >1m from the initial cut, to remove embolized xylem conduits. The cut segment was subsampled for NSC analysis. A-C_i curves were measured using the same portable gas exchange systems used for diurnal gas exchange measurement as described previously (Rogers et al. 2017c).

The same target tree species were measured for various hydraulic traits during the 2016 dry season, but independent of the diurnal measurement campaigns. Maximum stem area-specific hydraulic conductivity (Ks_{max}, Kg s^{-1} MPa^{-1} m^{-1}) and the water potential at 50% loss of stem hydraulic conductivity (P_{50}, MPa) were derived from measurements of terminal branches collected from canopy trees of each species following the bench-top dehydration method of Wolfe et al. (2016). P_{50} was calculated by plotting native stem-area specific hydraulic conductivity as a function of stem water potential and fitting a Weibull curve through the 90% percentile of with quantile regression. Ks_{max} was calculated as the intercept of the equation

described for P_{50}. Leaf turgor loss point (Ψ_{TLP}, MPa) was calculated from two to six pressure volume curves per species following Koide et al. (1989), except that leaf water potential was measured on leaf discs with a leaf cutter psychrometer (J.R.D. Merrill Specialty Equipment, Logan, Utah, USA). Maximum and minimum branch water potentials ($\Psi_{bmin,}$ Ψ_{bmax}, MPa) were measured with a pressure chamber at pre-dawn and midday, respectively, on leaves that were bagged since predawn (at least 1 h before measurement) and covered with reflective foam insulation to prevent overheating.

Additional measurements included ratio of leaf area to xylem area (A_l:A_x, m^2 m^{-2}), and densities of bark (WD_b, g cm^{-3}), xylem (WD_x, g cm^{-3}), and whole stem (WD_{ws}, g cm^{-3} including pith, xylem, and bark). We measured A_l:A_x on three to five branches of each species that were ~2m long and 19.4 ± 4.9 mm diameter at their base. Xylem area was measured with calipers (excluding bark and pith) and leaf area was measured with an area meter (LI-3100C, LI-COR, Lincoln, NE, USA). WD was measured on samples of the same terminal branches. After removing pith and bark, the fresh volume of wood samples was measured with water displacement on a digital balance and dry mass was measured after drying samples for >72 hours at 65 °C.

Non-structural Carbohydrate Analysis

Nonstructural carbohydrates are defined here as free, low molecular weight sugars (glucose, fructose, and sucrose) plus starch. Within two hours of collection, samples were microwaved at 600 watts for 90 s to stop enzymatic activity before drying at 60 °C for 48hrs. Leaf tissues were ball-milled to a fine powder (High Throughput Homogenizer, VWR International, Radnor, PA, USA). Woody tissues were ground with a Wiley Mini Mill (Thomas

Scientific, Inc., Swedesboro, NJ, USA) prior to ball-milling. Samples were analyzed following the protocol described by Hoch et al. (2002) modified for use with ethanol extraction (Landhäusser et al. 2018), and are not subject to inter-lab comparison errors (Quentin et al. 2015).

Fine ground plant material was extracted three times with 80% ethanol for 10 min. in a 90 °C water bath (Isotemp 105, Fisher Scientific International, Inc., Hampton, NH, USA). Ethanol was evaporated from the supernatant in a 50 °C oven overnight then reconstituted with DI water in a 90 °C water bath and centrifuged (Allegra X-15R, Beckman Coulter, Inc., Brea, CA, USA) for sugar quantification via enzymatic assay. The ethanol-insoluble pellet was dried at 50 °C overnight to remove residual ethanol and subsequently used for starch digestion and quantification.

Soluble sugars (glucose, fructose, sucrose) and starch were quantified by enzymatic assay (dataset available online, Dickman et al. 2018). For soluble sugar determination, sucrose in the reconstituted extract was first hydrolysed to glucose and fructose by incubation with invertase (Grade VII, from Baker's yeast, Sigma-Aldrich Co., St. Louis, MO, USA) for 40mins on a microplate shaker. The invertase-treated sample was then incubated on a microplate shaker (BioShaker M.BR-022UP, TAITEC) for 45 min. with phosphoglucose isomerase (from Baker's yeast – Type III, Sigma-Aldrich Co., St. Louis, MO, USA), glucose hexokinase and glucose-6-P dehydrogenase (Glucose Assay Reagent, Sigma-Aldrich Co., St. Louis, MO, USA), to convert fructose to glucose and glucose to gluconate-6-phosphate. The concentration of free glucose in a sample was determined photometrically in a 96-well microplate spectrophotometer (ELx800UV, BioTek Instruments, Inc., Winooski, VT, USA), relative to glucose standards of known

concentration, by the increase in optical density at 340nm resulting from the reduction of NAD+ to NADH as glucose-6-P is oxidized.

Starch was converted into soluble oligosaccharides and then to glucose using a two-step enzymatic digestion to avoid non-specific hydrolysis of non-starch polysaccharides (Denison et al. 1990). In the first step, starch in the ethanol-insoluble pellet was hydrolyzed to water soluble glucans using α-amylase from *Bacillus licheniformis*, (Sigma-Aldrich cat. no. A4551) at 85°C for two hours. After centrifugation, the glucans contained in the supernatant were converted to glucose using amyloglucosidase from *Aspergillus niger* (Sigma-Aldrich cat. no. 10115-5G-F) at 55°C for two hours. Following incubation, an aliquot of supernatant was used for photometric quantification of glucose hydrolysate as described above.

Statistical analyses

For all tests detailed below, NSC data were log or square root transformed to meet assumptions of normality. NSC values of zero were excluded because we were interested in evaluating changes in NSC when present, as opposed to presence vs. absence (note that statistical analyses were also peformed with zeros included as values of 0.001, and no conclusions changed). We first tested diurnal change in leaf NSCs using data from March, which included all times of day (early, mid, late) at all three sites. Data were analyzed using linear mixed effects models with site and time of day as fixed effects, sample ID nested within species as a random effect, and a corAR1 temporal autocorrelation structure for time of day. The likelihood ratio test was used to compare models with and without the random effect and temporal autocorrelation, and selection of the most parsimonious model was confirmed using AICc model selection. As recommended by Zuur et al. (2009), restricted maximum likelihood (REML) was used to

compare random structures, maximum likelihood was used to compare fixed structures (ML), and REML was used to evaluate the final model.

Leaf NSCs were found to increase over the course of the day (Fig. S1; Tables S5, S6; consistent with Würth et al. 1998), so the late time point (late-afternoon) – as an integration of daily leaf NSC assimilation – was used for all subsequent analyses (major conclusions did not change when the early timepoint or daily average were used instead). We next tested changes in leaf and branch NSCs across months with site and month as fixed effects, sample ID nested within species as a random effect, and a corAR1 temporal autocorrelation structure for month using the same model selection approach. When significant according to the likelihood ratio test, month was included as a random effect in subsequent analyses (i.e. for tests of species differences and trait relationships). Testing site and month effects on branch NSCs individually (i.e. site differences with March only, and month differences with SLZ only) had no significant impact on results (Tables S7, S8, S9). We next tested differences in leaf and branch NSCs between species with species as a fixed effect and site as a random effect, or month and sample ID nested within site as random effects with a corAR1 temporal autocorrelation structure for month when month was found to be significant in the previous analysis. We finally tested the relationships between leaf and branch NSCs and various leaf and hydraulic traits with traits as fixed effects and species as a random effect, or month and species as a random effects with a corAR1 temporal autocorrelation structure for month when month was previously found to be significant. For post-hoc analysis of significant fixed effects, we used a general linear hypothesis test with Tukey's honest significant difference. We used R (R Core Team, 2017) with *nlme* (Pinheiro et al., 2017) and *multcomp* (Hothorn T, F. Bretz & P.Westfall, 2008) to perform all analyses.

Results

Leaf NSCs increased over the course of the day (Fig. S1) driven by both starch and soluble sugar accumulation (Tables S5, S6). Due to this diurnal trend, we used the late afternoon time point for all further analyses as it was the most representative of carbohydrate accumulation over the day, and it was the diurnal time point for which we had the most complete dataset. Both leaf and branch total NSCs were invariant over the course of the drought (Fig. 2a, S2a, Tables S7, S10), suggesting that NSC sources (photosynthates) and sinks (growth and metabolism) were balanced throughout the dry period. Leaf and branch total NSCs were also invariant across sites (Fig. 3, S3a, Tables S7, S11) despite the substantial gradient in mean annual precipitation (Table 1). Despite these observed constancies, there were some changes associated with drought. Most notably, leaf NSC composition shifted from soluble sugars to starch throughout the dry period (Fig. 2b-d, Tables S7, S10), and branch soluble sugars were higher at the driest site (Fig S3d, Tables S7, S11).

The high variability in NSCs observed across species (Fig. 4, Table S12) could be partially predicted by structural and leaf traits (Figs. 6, 7, S1, Tables S1, S13). Leaf total NSCs were positively related to LMA (Fig. 5, Table S13), while branch soluble sugars were negatively related to leaf level photosynthesis (using the mean daily photosynthetic rate) and xylem wood density (Fig. 6a, b, Table S13), and positively related to leaf temperature (Fig. 6c, Table S13). Branch starch increased exponentially with turgor loss point (Fig. S4, Table S13). The other traits tested, including parameters such as stomatal conductance (g_s), leaf water potential (Ψ_{leaf}), maximum carboxylation rate (V_{cmax}), and stem water potential at 50% loss of hydraulic conductivity (P_{50}) (Table S1), showed no significant relationships with NSCs. We also included

303 drought sensitivity metrics (Table S2), such as the difference between pre-dawn and mid-day leaf
304 water potential ($\Delta\Psi$) and the slope of the relationship between pre-dawn and mid-day leaf water
305 potential (slope Ψ_{PD}: Ψ_{MD}; Figs. S5, S6, Tables S2, S13). Despite wide species variation in these
306 parameters we found poor fits to the NSC observations.

307

308 **Discussion**

309 We tested the hypothesis that NSCs would increase during the drought progression but be
310 maintained at relatively constant, or homeostatic, levels under long-term (across site) variation in
311 precipitation. These hypotheses were tested across communities located along a large
312 precipitation gradient during the drought imposed by the 2015-2016 El Niño. Despite large
313 variation in NSCs across species (Fig. 4, Table S12), we found total NSC content of foliage and
314 branches was held relatively homeostatic both across the drought period and across the
315 precipitation gradient (Figs. 2a, 3, S2a, S3a; Tables S7, S10, S11). Traits explained some, but not
316 all, of the observed variation in NSCs across species (Figs. 5, 6, S1, Table S13).

317 Leaf and branch total NSCs were maintained both over the course of the 2016 dry period
318 when we made our measurements (Fig. 2a, S2a; Tables S7, S10), and across the precipitation
319 gradient (Fig. 3, S3a; Tables S7, S11). This homeostasis suggests that NSCs serve an important
320 function and are preserved as a priority carbon sink (Chapin et al. 1990, Dietze et al. 2014,
321 Martinez-Vilalta et al. 2016). This result is consistent with previous studies in which NSC
322 concentrations have been found to be relatively resistant to change under all but the most
323 extreme conditions. Variation in temperature and moisture have been shown to have modest
324 impacts on NSC concentrations over seasonal (Martinez-Vilalta et al. 2016) and decadal time-

scales (Rowland et al. 2015; Schoenbeck et al. 2018), with only the most severe conditions that result in plant death causing larger NSC declines (Adams et al. 2017). The mechanisms driving such homeostatic balance of NSCs against large changes in short- and long-term precipitation are unknown, but include shifts in NSC consumption, e.g. to growth, defense, and energy production, that match any shifts in photosynthesis during drought (McDowell 2011). The homeostatic maintenance of leaf total NSCs throughout the seasonal drought in this study was associated with a shift from soluble sugars to starch (Fig. 2b-d; Tables S7, S10), suggesting either drought-constrained limitations on foliar metabolism and growth (Würth et al. 2005) resulting in increased storage as drought progressed (McDowell 2011), or prioritization of foliar storage over other processes during drought (Hartmann et al. 2015). The latter process is consistent with the idea that these plants have experienced worse droughts (e.g. Condit et al. 1996), and may have adapted to maintain relatively high NSCs in case of an extremely prolonged or severe drought (Wright 2005). Such adaptation could come in the form of shifts in uptake or allocation of carbon that induce such homeostatic patterns. In contrast to leaves, branch soluble sugars were higher and starch trended lower at the dry than the wet site (Fig. S3) which may be related to a greater need for soluble sugars for embolism repair under drier conditions (Secchi et al. 2011). The longer term response (across site) in branches and shorter term response (with ENSO drought progression) in leaves is consistent with the transitory nature of carbohydrate pools in leaves relative to branches.

Our observed relationships between NSCs and traits may serve to simplify both modeling of carbon storage and collection of benchmark data, and emphasizes the importance of trait-based modeling (van Bodegom et al. 2014) to capture species-level differences in NSCs. Our observation of a positive relationship between leaf mass per area and foliar NSCs (Fig. 5, Table

S13) is consistent with an increase in leaf dry mass as sugars accumulate (Poorter et al. 2009). Interestingly, branch soluble sugars were correlated with several metrics, including average photosynthetic rate on the day of NSC sampling, xylem wood density, and leaf temperature (Fig. 6, Table S13). The negative relationship between branch soluble sugars and photosynthesis (Fig. 6a, Table S13) may be the result of feedback inhibition, whereby reduced sink strength and phloem transport resulting from higher branch soluble sugars promotes a reduction in photosynthetic rate (Paul & Foyer 2001, Thompson & Holbrook 2003, McCormick et al. 2009). The decrease in branch soluble sugars with increasing wood density (Fig. 6b, Table S13) has several possible explanations. Recent research has shown that increased sugar concentrations in woody tissues reduce xylem vulnerability to cavitation (De Baerdemaeker et al. 2017), and species with higher wood densities and therefore lower vulnerability (Hacke et al. 2001, Jacobsen et al. 2005) would require less soluble sugar for repair. There is also evidence that xylem parenchyma, the sugar transport and storage fraction in woody tissue that links the heartwood and phloem, is related to embolism recovery (Secchi et al. 2017). Alternatively, wood density is negatively correlated with phloem proportion in some species (Santini et al. 2012), so there may simply be less soluble sugar transport tissue associated with denser wood. There may also be a basic physical limitation whereby higher structural density reduces the space available for sugar storage. Branch soluble sugars were also positively related to leaf temperature (Fig. 6c, Table S13). This finding is contrary to research showing inhibition of assimilate export with increased leaf temperature (Jiao & Grodzinski 1996). However Jiao & Grodzinski also show declines in photosynthesis with leaf temperature (1996) which is consistent with the observed negative relationship between branch soluble sugars and photosynthesis (Fig. 6a, Table S13) discussed above. In our case, there was no observed correlation between photosynthesis and

leaf temperature across species ($r^2 = 0.14$). However, leaf temperature was consistently higher at the driest site compared to the wettest site (Fig. S7), which may explain the site differences in branch soluble sugars (PNM>SLZ; Fig. S3d).

Despite these few correlations, we did not find expected relationships between NSCs and drought sensitivity or hydraulic metrics (Figs. S5, S6; Tables S1, S2), including leaf water potential (Fig. S8), hydraulic conductivity, and P_{50}. Though increased leaf soluble sugars are often associated with more negative water potentials (e.g. Dickman et al. 2014), these trees may not have experienced dry enough conditions to necessitate osmotic regulation. We also explored relationships with relative degree of isohydry (Fig. S5, Martinez-Villalta et al. 2014), yet there was no significant correlation to NSCs (Fig. S6a) despite target species ranging from extreme isohydry to extreme anisohydry (Fig. S6b, Table S2). Similarly, we found no correlation between NSCs and $\Delta\Psi$, or difference between pre-dawn and mid-day leaf water potential (Table S2). This absence of relationships across many functional traits, particularly hydraulic traits, further emphasizes the homeostatic nature of NSCs in this system, that is, NSCs are relatively invariant across a wide spectrum of hydraulic traits across the Ithmus of Panama; at least for the canopy tree species explored here. To the extent that the natural rainfall gradient is a proxy for adaptation to long term precipitation changes (specifically decreasing mean annual precipitation), this suggests that NSCs will also be held homeostatic under future potentially drier conditions, though manipulative studies (e.g. Rowland et al. 2015) are best utilized to test this hypothesis. We note that many hydraulic metrics exist that we did not test (e.g. vulnerability to embolism, Choat et al. 2012) that may provide more insight into regional patterns of NSC regulation.

Our results suggest that, despite broad species diversity, NSCs in tropical canopy trees are maintained homeostatically at the community level through a seasonal and ENSO-influenced drought, across a long-term climatic gradient, and across a wide variety of functional traits. We cannot exclude the possibility that more exceptional droughts, particularly with increased dry down of soil moisture, could cause depletions of NSC in these tropical forests. However, these observations indicate that maintenance of NSCs is prioritized, and may simplify our ability to represent NSC dynamics in next-generation Earth Systems Models, which currently use carbon storage as a proxy to simulate tree mortality (e.g., Fisher et al 2010; McDowell et al. 2013).

Acknowledgements

This work was supported by the Next-Generation Ecosystem Experiments, Tropics project funded by the U.S. Department of Energy, Office of Science, Biological and Environmental Research, and through contract #DE-SC0012704 to Brookhaven National Laboratory.

References

Allan R., J. Lindsay, & D. Parker (1996) El Niño Southern Oscillation and Climate Variability, CSIRO, Melbourne, Vic., Australia.

Adams HD, Zeppel MJB, WRL Anderegg, H Hartmann, SM Landhäusser, DT Tissue,…, McDowell NG (2017) A multi-species synthesis of physiological mechanisms in drought-induced tree mortality. Nature Ecology & Evolution 1:1285–1291.

Basset, Y., V. Horlyck and SJ Wright, editors. 2003. Studying Forest Canopies from Above: The International Canopy Crane Network. Imprenta Boski, S. A., Panama. 196 pp. (ISBN 9962-614-05-8).

Beer C, Reichstein M, Tomelleri E, Ciais P, Jung M, Carvalhais N,..., Papale D (2010) Terrestrial gross carbon dioxide uptake: global distribution and covariation with climate. Science 329: 834–838.

Blonder B., Michaletz ST (2018) A model for leaf temperature decoupling from air temperature. Agricultural and Forest Meteorology 262:354-36.

Cai W, Borlace S, Lengaigne M, van Rensch P, Collins M, Vecchi G, Timmermann A, Santoso A, McPhaden MJ, Wu L, England MH, Wang G, Guilyardi E, and Jin F-F (2014) Increasing frequency of extreme El Niño events due to greenhouse warming Nature Climate Change 4: 111–116.

Cavaleri, M. A., Coble, A. P., Ryan, M. G., Bauerle, W. L., Loescher, H. W. and Oberbauer, S. F. (2017), Tropical rainforest carbon sink declines during El Niño as a result of reduced photosynthesis and increased respiration rates. New Phytol, 216: 136-149. doi:10.1111/nph.14724.

Chapin III F.S., Schulze E.D. and Mooney H.A. (1990) The ecology and economics of storage in plants. Annual review of ecology and systematics, 21(1), pp.423-447.

Choat, B., Jansen, S., Brodribb, T.J., Cochard, H., Delzon, S., Bhaskar, R., et al. (2012) Global convergence in the vulnerability of forests to drought. Nature, 491, 752–755.

Condit R, Hubbell SP, & Foster RB (1996) Changes in tree species abundance in a neotropical forest: impact of climate change. Journal of Tropical Ecology 12, 231–256.

De Baerdemaeker N. J., Salomón R. L., De Roo L. & Steppe K. (2017), Sugars from woody tissue photosynthesis reduce xylem vulnerability to cavitation. New Phytologist, 216: 720-727.

Detto, M., Wright, S. J., Calderón, O., & Muller-landau, H. C. (2018). Resource acquisition and reproductive strategies of tropical forest in response to the El Niño-Southern Oscillation. Nature Communications, 9(913), 1–8. https://doi.org/10.1038/s41467-018-03306-9.

Dickman L.T., N.G. McDowell, S. Sevanto, R.E. Pangle, W.T. Pockman (2014). Carbohydrate dynamics and mortality in a pinyon–juniper woodland under three future precipitation scenarios. Plant Cell Environ, 38, pp. 729-739.

Dickman T; Ely K; Rogers A; Serbin S; Wu J; Wolfe B; Collins A; Detto M; Grossiord C; McDowell N; Michaletz S (2018): 2016 Panama ENSO Non-Structural Carbohydrates (NSC), Feb2016-May2016, PA-SLZ, PA-PNM, PA-BCI. 1.0. NGEE Tropics Data Collection. (dataset). http://dx.doi.org/10.15486/ngt/1478647.

Dietze MC, Sala A, Carbone MS, Szimczik CI, Mantooth JA, Richardson AD, Vargas R (2014) Nonstructural carbon in woody plants. Annual Review of Plant Biology 65:667–687.

Ehleringer J. R. & Cerling T. E. (1995) Atmospheric CO2 and the ratio of intercellular to ambient CO2 concentrations in plants. Tree Physiology 15: 105–111.

Ely K; Rogers A; Serbin S; Wu J; Wolfe B; Dickman T; Collins A; Detto M; Grossiord C; McDowell N; Michaletz S (2018): Leaf mass area, Feb2016-May2016, PA-SLZ, PA-PNM, PA-BCI: Panama. 1.0. NGEE Tropics Data Collection. (dataset). http://dx.doi.org/10.15486/ngt/1411973.

Fisher, R. N.G. McDowell, D. Purves, P. Moorcroft, S. Sitch, P. Cox, C. Huntingford, P. Meir, I. Woodward. 2010. Assessing uncertainties in a second-generation dynamic vegetation model due to ecological scale limitations. New Phytologist, 187:666-681.

Hacke UG, Sperry JS, Pockman WT, Davis SD, McCulloh KA (2001) Trends in wood density and structure are linked to prevention of xylem implosion by negative pressure. Oecologia 126: 457–461.

Hartmann H, McDowell NG, Trumbore S (2015) Allocation to carbon storage pools in Norway spruce saplings under drought and low CO2. Tree Physiology 35(3): 243–252.

Heldt (2005) Plant Biochemistry. Third Edition. Elsevier. https://doi.org/10.1016/B978-0-12-088391-2.X5000-7.

Hoch G., Popp M. & Ko¨rner C. (2002) Altitudinal increase of mobile carbon pools in Pinus cembra suggests sink limitation of growth at the Swiss treeline. Oikos 98: 361–374.

Hothorn T, F. Bretz & P.Westfall (2008). Simultaneous Inference in General Parametric Models. Biometrical Journal 50(3), 346--363.

IPCC, 2013: Climate Change 2013: The Physical Science Basis. Contribution of Working Group I to the Fifth Assessment Report of the Intergovernmental Panel on Climate Change [Stocker, T.F., D. Qin, G.-K. Plattner, M. Tignor, S.K. Allen, J. Boschung, A. Nauels, Y. Xia, V. Bex and P.M. Midgley (eds.)]. Cambridge University Press, Cambridge, United Kingdom and New York, NY, USA, 1535 pp.

Jacobsen AL, Ewers FW, Pratt RB, Paddock WA, & Davis SD. (2005) Do xylem fibers affect vessel cavitation resistance? Plant Physiology 139:546–556.

Jiao J & B Grodzinski. (1996) The effect of leaf temperature and photorespiratory conditions on export of sugars during steady-state photosynthesis in Salvia splendens. Plant physiology 111(1):169-178.

Körner, C. (2003). Carbon limitation in trees. Journal of Ecology 91, 4–17. doi: 10.1046/j.1365-2745.2003.00742.x

Landhäusser SM, Chow PS, Dickman LT, Furze M, Kuhlman I, Schmid S,…, Adams HD. 2018 Standardized protocols and procedures can precisely and accurately quantify non-structural carbohydrates. Tree Physiology, tpy118, https://doi.org/10.1093/treephys/tpy118.

Latt C.R, Nair P.K.R, Kang B.T (2001) Reserve carbohydrate levels in the boles and structural roots of five multipurpose tree species in a seasonally dry tropical climate. Forest Ecology and Management, 146:1–3 (145-158).

Laurance, W. F. and Williamson, G. B. (2001) Positive feedbacks among forest fragmentation, drought, and climate change in the Amazon. Conservation Biology, 15: 1529-1535.

491 Li, X., Xiao, J. and He, B., 2018. Higher absorbed solar radiation partly offset the negative
492 effects of water stress on the photosynthesis of Amazon forests during the 2015 drought.
493 Environmental Research Letters, 13(4), p.044005.
494 Martínez-Vilalta J., Poyatos R., Aguadé D., Retana J. and Mencuccini M. (2014), A new look at
495 water transport regulation in plants. New Phytologist, 204: 105-115.
496 Martínez-Vilalta J., Sala A., Asensio D, Galiano L., Hoch G. , Palacio S., Piper F. I. and Lloret,
497 F. (2016) Dynamics of non-structural carbohydrates in terrestrial plants: a global
498 synthesis. Ecological Monographs, 86: 495-516.
499 McCormick A. J., D. A. Watt and M. D. Cramer (2009) Supply and demand: sink regulation of
500 sugar accumulation in sugarcane. Journal of Experimental Botany 60(2): 357–364.
501 McDowell N.G., Adams H.D., Bailey J.D., Hess M. and Kolb T.E. (2006). Homeostatic
502 maintenance of ponderosa pine gas exchange in response to stand density changes.
503 Ecological Applications, 16(3), pp.1164-1182.
504 McDowell, N.G. (2011). Mechanisms linking drought, hydraulics, carbon metabolism, and
505 vegetation mortality. Plant Physiology 155: DOI 10.1104/pp.110170704
506 McDowell NG, Fisher RA, Xu C, Domec JC, Hölttä T, Mackay DS, Sperry JS, Boutz A,
507 Dickman L, Gehres N, Limousin JM, Macalady A, Martinez-Vilálta J, Mencuccini M,
508 Plaut JA, Ogee J, Pangle RE, Rasse DP, Ryan MG, Sevanto S, Waring RH, Williams
509 AP, Yepez EA, Pockman WT. (2013). Evaluating theories of drought-induced vegetation
510 mortality using a multi-model-experiment framework. New Phytologist 200(2), 304-321
511 Michaletz ST, Weiser MD, Zhou J, Kaspari M, Helliker BR, Enquist BJ. 2015. Plant
512 thermoregulation: Energetics, trait-environment interactions, and carbon economics.
513 Trends in Ecology & Evolution 30:714-724.

514 Michaletz ST, Weiser MD, McDowell NG, Zhou J, Kaspari M, Helliker BR, Enquist BJ. 2016.
515 The energetic and carbon economic origins of leaf thermoregulation. Nature Plants
516 2:16129.
517 Myers, J. A. and Kitajima, K. (2007) Carbohydrate storage enhances seedling shade and stress
518 tolerance in a neotropical forest. Journal of Ecology, 95: 383-395.
519 Nagai S, Ichii K, & Morimoto H (2007) Interannual variations in vegetation activities and
520 climate variability caused by ENSO in tropical rainforests. International Journal of
521 Remote Sensing 28(6): 1285-1297.
522 Nani Li, Nianpeng He, Guirui Yu, Qiufeng Wang, Jian Sun (2016) Leaf non-structural
523 carbohydrates regulated by plant functional groups and climate: Evidences from a
524 tropical to cold-temperate forest transect. Ecological Indicators, 62: 22-31.
525 Newell E.A., Mulkey S.S. & Wright J.S. (2002) Seasonal patterns of carbohydrate storage in
526 four tropical tree species. Oecologia, 131: 333.
527 O'Brien MJ, Leuzinger S, Philipson CD, Tay J, Hector A. 2014. Drought survival of tropical tree
528 seedlings enhanced by non-structural carbohydrate levels. Nature Climate Change, 4:
529 710–714.
530 Pan Y, Birdsey RA, Phillips OL, Jackson RB. 2013. The structure, distribution, and biomass of
531 the world's forests. Annual Review of Ecology, Evolution, and Systematics 44: 593–622.
532 Paul, M. J., & Foyer, C. H. (2001). Sink regulation of photosynthesis. Journal of Experimental
533 Botany, 52(360), 1383–1400. https://doi.org/10.1093/jexbot/52.360.1383.
534 Pinheiro J, Bates D, DebRoy S, Sarkar D and R Core Team (2017). nlme: Linear and Nonlinear
535 Mixed Effects Models. R package version 3.1-131, https://CRAN.R-
536 project.org/package=nlme.

Poorter, L. and Kitajima, K. (2007), Carbohydrate storage and light requirements of Tropical moist and dry forest tree species. Ecology, 88: 1000-1011.

Poorter, H. , Niinemets, Ü. , Poorter, L. , Wright, I. J. and Villar, R. (2009), Causes and consequences of variation in leaf mass per area (LMA): a meta-analysis. New Phytologist, 182: 565-588.

Poorter, L. , Kitajima, K. , Mercado, P. , Chubiña, J. , Melgar, I. and Prins, H. H. (2010), Resprouting as a persistence strategy of tropical forest trees: relations with carbohydrate storage and shade tolerance. Ecology, 91: 2613-2627.

Rogers A, Allen DJ, Davey PA, Morgan PB, Ainsworth EA, Bernacchi CJ, Cornic G, Dermody O, Heaton EA, Mahoney J, Zhu X-G, DeLucia EH, Ort DR, Long SP (2004) Leaf photosynthesis and carbohydrate dynamics of soybeans grown throughout their life-cycle under Free-Air Carbon dioxide Enrichment. Plant Cell & Environment. 27, 449-458.

Rogers A; Serbin S; Ely K; Wu J; Wolfe B; Dickman T; Collins A; Detto M; Grossiord C; McDowell N; Michaletz S (2017a): Diurnal leaf gas exchange survey, Feb2016-May2016, PA-SLZ, PA-PNM: Panama. 1.0. NGEE Tropics Data Collection. (dataset). http://dx.doi.org/10.15486/ngt/1411972.

Rogers A; Serbin S; Ely K; Wu J; Wolfe B; Dickman T; Collins A; Detto M; Grossiord C; McDowell N; Michaletz S (2017b): CO2 response (ACi) gas exchange, calculated Vcmax & Jmax parameters, Feb2016-May2016, PA-SLZ, PA-PNM: Panama. 1.0. NGEE Tropics Data Collection. (dataset). http://dx.doi.org/10.15486/ngt/1411867.

Rogers, A., S. P. Serbin, K. S. Ely, V. L. Sloan, and S. D. Wullschleger. 2017c. Terrestrial biosphere models underestimate photosynthetic capacity and CO_2 assimilation in the Arctic. New Phytologist 216:1090-1103.

560 Rowland L, A.C.L. da Costa, D.R. Galbraith, R.S. Oliveira, O.J. Binks, A.A.R. Oliveira, …, P.
561 Meir. (2015) Death from drought in tropical forests is triggered by hydraulics not carbon
562 starvation. Nature, 528: 119–122.
563 Santini, N.S., Schmitz, N. & Lovelock, C.E. (2012) Variation in wood density and anatomy in a
564 widespread mangrove species. Trees, 26: 1555.
565 Schönbeck L., Gessler A., Hoch G., McDowell N. G., Rigling A., Schaub M. and Li M. (2018)
566 Homeostatic levels of nonstructural carbohydrates after 13 yr of drought and irrigation in
567 Pinus sylvestris. New Phytologist. doi:10.1111/nph.15224.
568 Saatchi S, Asefi-Najafabady S, Malhi Y, Aragão L, Anderson L., Myneni R, Nemani R. 2013.
569 Persistent effects of a severe drought on Amazonian forest canopy. Proceedings of the
570 National Academy of Sciences, 110 (2) 565-570; DOI: 10.1073/pnas.1204651110.
571 Secchi, F., Gilbert, M. E., & Zwieniecki, M. A. (2011). Transcriptome Response to Embolism
572 Formation in Stems of Populus trichocarpa Provides Insight into Signaling and the
573 Biology of Refilling. Plant Physiology, 157(3), 1419–1429.
574 http://doi.org/10.1104/pp.111.185124.
575 Secchi F, C Pagliarani & MA. Zwieniecki. (2017) The functional role of xylem parenchyma cells
576 and aquaporins during recovery from severe water stress. Plant, Cell and Environment,
577 40, 858–871.
578 Thompson, M. V., & Holbrook, N. M. (2003). Application of a single-solute non-steady-state
579 phloem model to the study of long-distance assimilate transport. Journal of Theoretical
580 Biology, 220(4), 419–455. https://doi.org/10.1006/jtbi.2003.3115.

581 Tian H., JM. Melillo, DW. Kicklighter, A.D McGuire, JVK. Helfrich III, B Moore III & CJ.
582 Vörösmarty (1998) Effect of interannual climate variability on carbon storage in
583 Amazonian ecosystems. Nature 396, 664–667.
584 van Bodegom P.M., J.C. Douma, L.M. Verheijen. (2014) A fully traits-based approach to
585 modeling global vegetation distribution. PNAS 111 (38) 13733-13738.
586 Wolfe, B.T., Sperry, J.S., & Kursar, T.A. 2016. Does leaf shedding protect stems from cavitation
587 during seasonal droughts? A test of the hydraulic fuse hypothesis. New Phytologist 212:
588 1007–1018.
589 Wolfe B; Wu J; Ely K; Serbin S; Rogers A; Dickman T; Collins A; Detto M; Grossiord C;
590 McDowell N; Michaletz S (2017): Leaf water potential, Feb2016-May2016, PA-SLZ,
591 PA-PNM, PA-BCI: Panama. 1.0. NGEE Tropics Data Collection. (dataset).
592 http://dx.doi.org/10.15486/ngt/1411970.
593 Wright, SJ 2005. The influence of the El Niño Southern Oscillation on tropical forests. Pages
594 295-310 in E. Bermingham, C. Dick and C. Moritz, editors. Rain forests: past, present
595 and future. University of Chicago Press, Chicago. 1004 pages.
596 Würth M., Winter K. & Körner C. (1998) Leaf carbohydrate responses to CO_2 enrichment at the
597 top of a tropical forest. Oecologia 116(1-2):18-25.
598 Würth M.K.R., Peláez-Riedl S., Wright S.J. & Körner C. (2005) Non-structural carbohydrate
599 pools in a tropical forest. Oecologia, 143(1):11-24.

Tables

Table 1: Site characteristics (1998-2015 mean). All three sites are characterized by a pronounced dry season (approximately from mid-December to the end of April), and a wet season (May to mid-December). Data provided by http://biogeodb.stri.si.edu/physical_monitoring/research/.

	PNM	BCI	SLZ
Location	8°58'N, 79°34'W	9°10'N, 79°51'W	9°17'N, 79°58'W
Elevation (m)	50	70	70
Annual Precip. (mm)	1844	2352	3282
Dry Season Precip. (mm)	210	308	655
Dry Season Solar Rad. (MJ m^{-2} d^{-1})	17	19	16
Wet Season Solar Rad. (MJ m^{-2} d^{-1})	13	14	13
Tmin (°C)	23	24	24
Tmax (°C)	31	30	28

Figure legends

Figure 1: Cumulative annual rainfall by site. Monthly field campaigns (vertical gray dashed lines) were conducted at three sites across the Isthmus of Panama throughout the 2016 dry season (mid-Feb to mid-May; see inset). The Parque Natural Metropolitano crane site on the Pacific coast (PNM, yellow - dry) and the San Lorenzo crane site on the Caribbean Sea (SLZ, blue - wet) were sampled each month. The Barro Colorado Island site in the Panama Canal (BCI, green - intermediate) was only sampled in March. Each campaign included diurnal measurement of leaf traits. Cumulative annual rainfall (2016 - solid lines; 1998-2015 mean - broken lines) was calculated from data provided by http://biogeodb.stri.si.edu/physical_monitoring/. Shaded regions indicate one standard deviation of the 1998-2015 mean.

Figure 2: Leaf total NSCs (a) don't change with drought duration, but ratio of leaf soluble sugars to starch (b) declines due to increased starch (c) and decreased soluble sugars (d). Data are from the late time point across all sites (PNM n = 18; BCI n = 15; SLZ n = 18). Error bars are standard errors. Letters indicate significant differences in log transformed NSC for soluble sugars:starch and starch, and square-root transformed NSC for soluble sugars.

Figure 3: No difference in leaf total NSCs across the precipitation gradient. Data are from the late time point. Error bars are standard errors.

Figure 4: Large variation in NSCs across species. Leaf data are from the late time point. Branch samples were collected at PNM in March and at SLZ in March and April. Branch samples were not collected at BCI due to lack of canopy access. Species are arranged by site from left to right: PNM, BCI, SLZ. Error bars are standard errors of total NSC. No error bars are shown for branches from PNM since there is only one sampling point.

Figure 5: Leaf mass per area explains some variation in leaf total NSCs. NSC data are from the late time point. Each point represents one species.

Figure 6: Branch soluble sugars are negatively related to photosynthesis and xylem wood density, and positively related to leaf temperature. Each point represents one species.

Figures

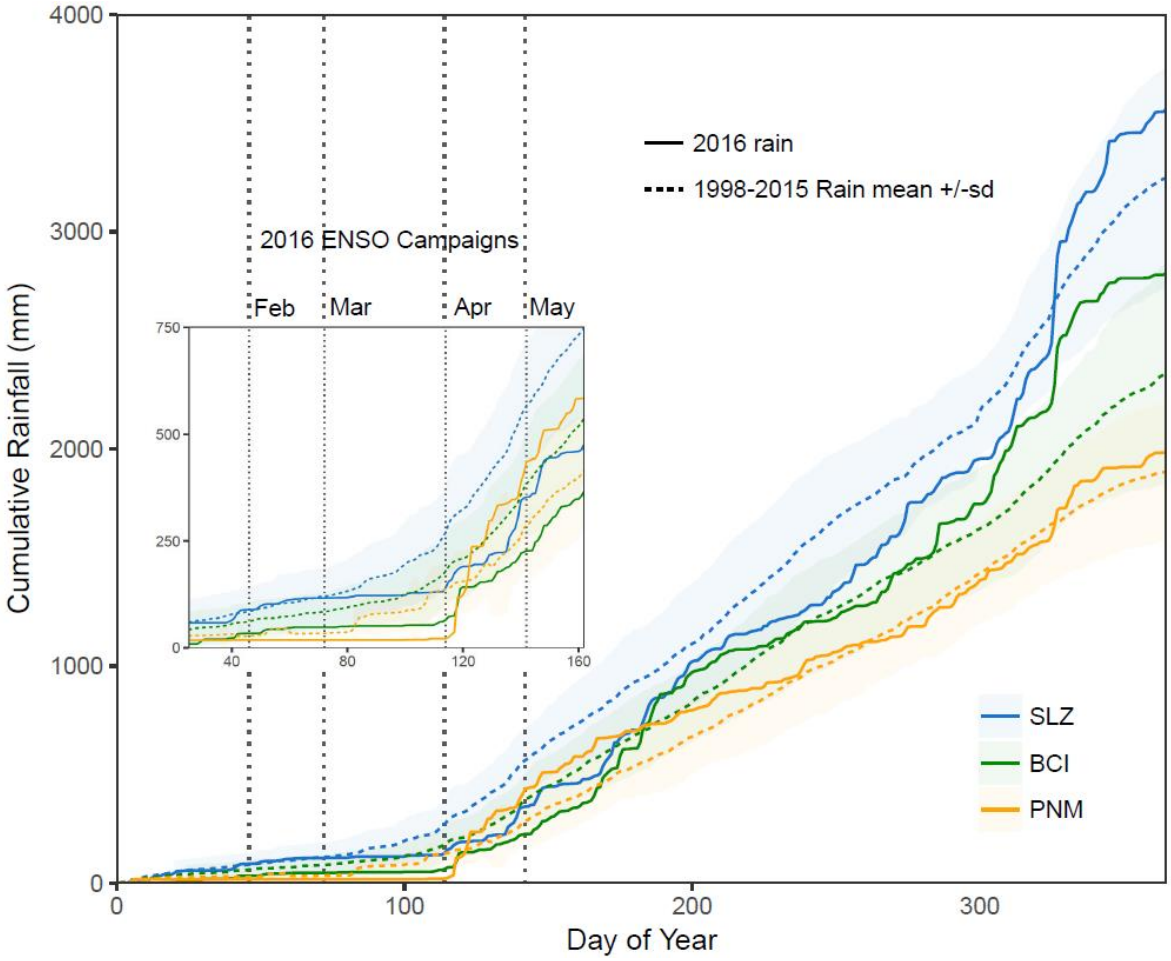

Figure 1: Cumulative annual rainfall by site. Monthly field campaigns (vertical gray dashed lines) were conducted at three sites across the Isthmus of Panama throughout the 2016 dry season (mid-Feb to mid-May; see inset). The Parque Natural Metropolitano crane site on the Pacific coast (PNM, yellow - dry) and the San Lorenzo crane site on the Caribbean Sea (SLZ, blue - wet) were sampled each month. The Barro Colorado Island site in the Panama Canal (BCI, green - intermediate) was only sampled in March. Each campaign included diurnal measurement of leaf traits. Cumulative annual rainfall (2016 - solid lines; 1998-2015 mean - broken lines) was calculated from data provided by http://biogeodb.stri.si.edu/physical_monitoring/. Shaded regions indicate one standard deviation of the 1998-2015 mean.

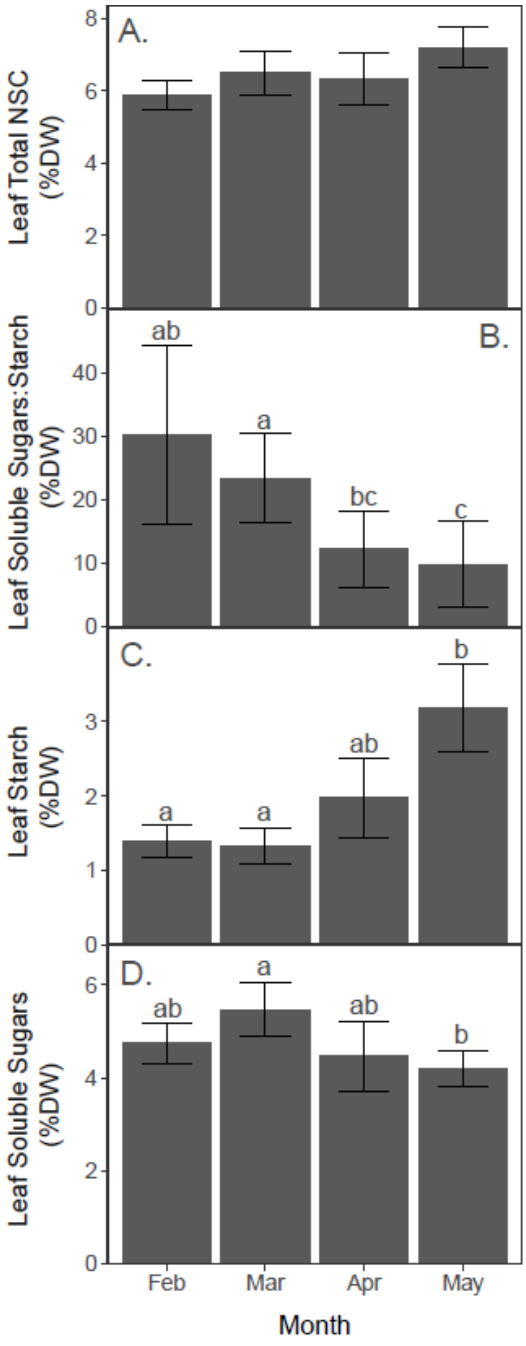

Figure 2: Leaf total NSCs (a) don't change throughout the drought, but ratio of leaf soluble sugars to starch (b) declines due to increased starch (c) and decreased soluble sugars (d). Data are from the late time point across all sites (PNM n = 18; BCI n = 15; SLZ n = 18). Error bars are standard errors. Letters indicate significant differences in log transformed NSC for soluble sugars:starch and starch, and square-root transformed NSC for soluble sugars .

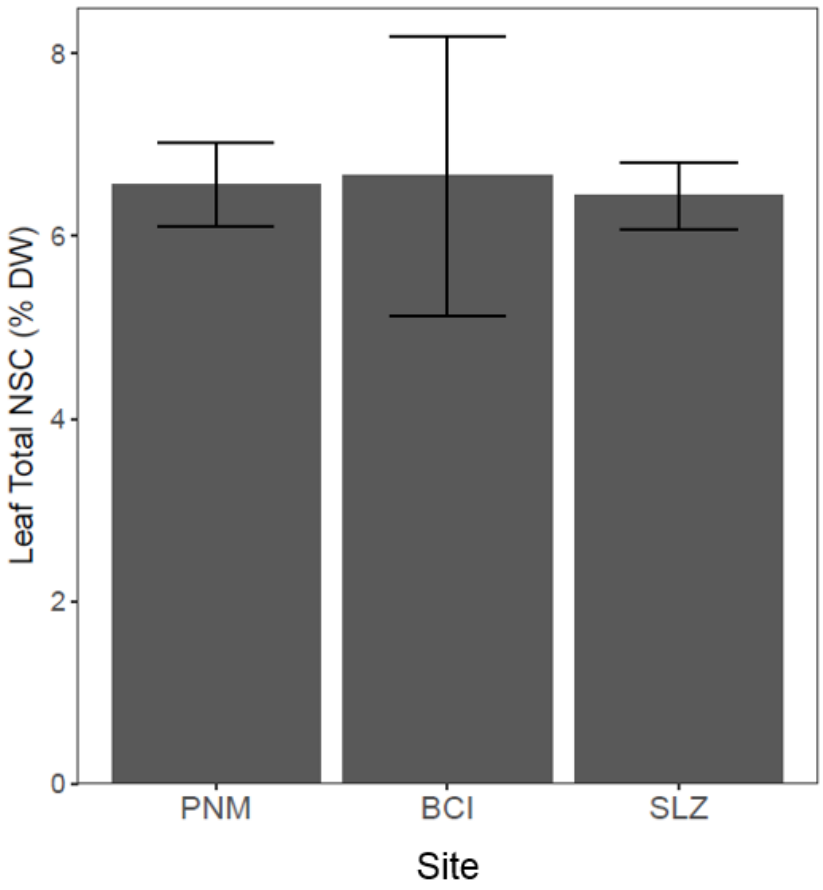

Figure 3: No difference in leaf total NSCs across the precipitation gradient. Data are from the late time point (PNM n = 54; BCI n = 15; SLZ n = 72). Error bars are standard errors.

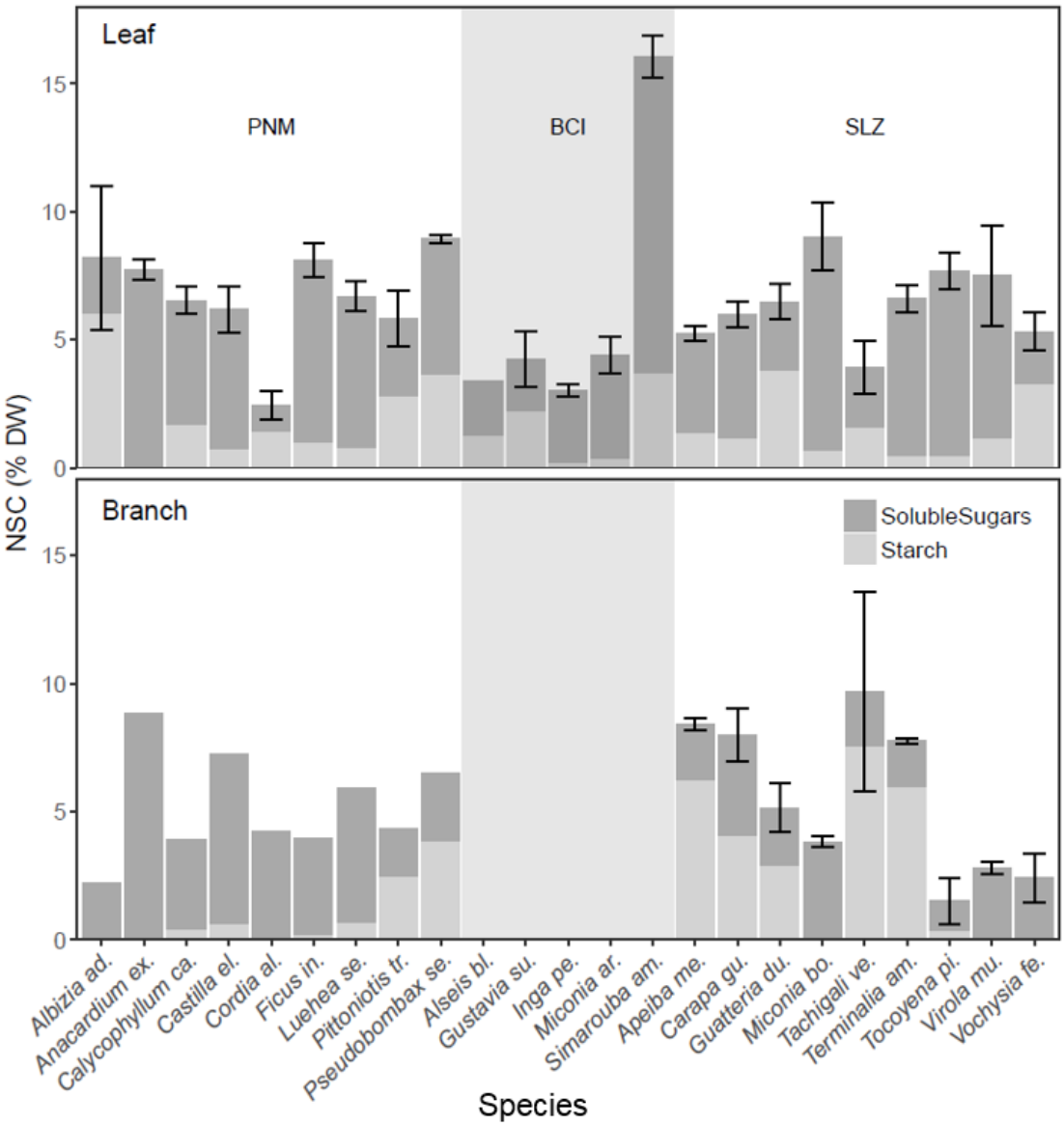

657

658 **Figure 4:** Large variation in NSCs across species. Leaf data are from the late afternoon time
659 point (PNM n = 6; BCI n = 3; SLZ n = 8). Branch samples were collected at PNM in March (n =
660 1) and at SLZ in March and April (n = 2). Branch samples were not collected at BCI due to lack
661 of canopy access. Species are arranged by site from left to right: PNM, BCI, SLZ. Dark shading
662 represents soluble sugars, light shading represents starch (see inset color key). Error bars are
663 standard errors of total NSC. No error bars are shown for branches from PNM since there is only
664 one sampling point.

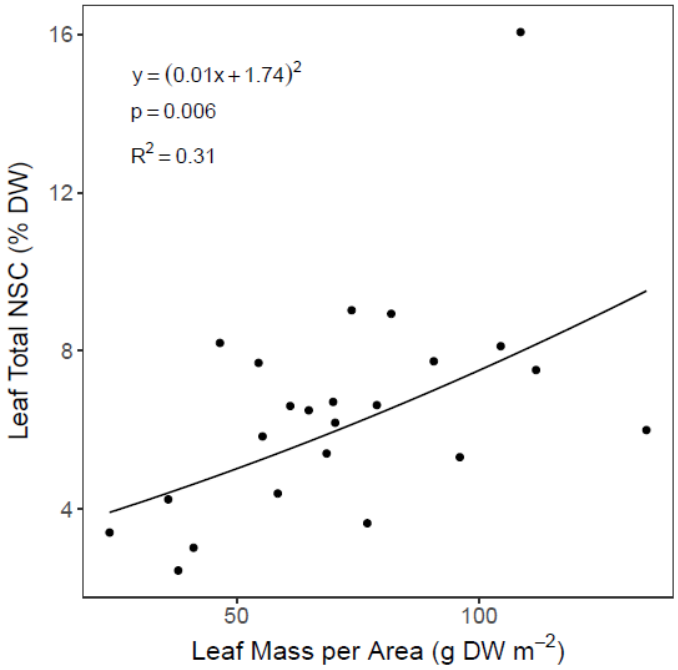

665

666 **Figure 5:** Leaf mass per area explains some variation in leaf total NSCs. NSC data are from the
667 late time point. Each point represents one species. The regression without the highest NSC point
668 remains significant but the correlation declines ($p=0.02$, $R^2=0.24$).

669

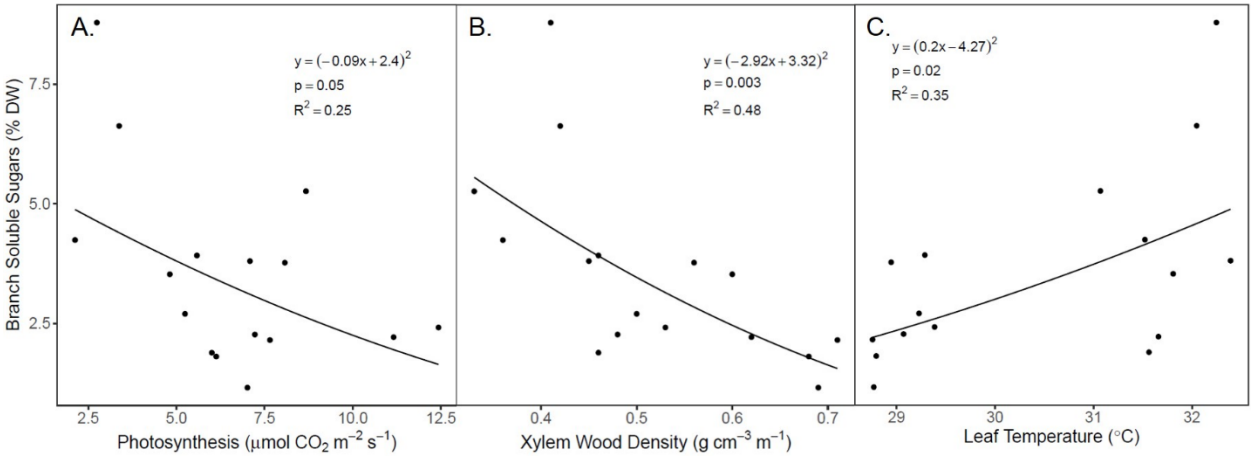

670

671 **Figure 6:** Branch soluble sugars are negatively related to mean daily photosynthesis and xylem
672 wood density, and positively related to leaf temperature. Each point represents one species.

673 **Supporting Information**

674

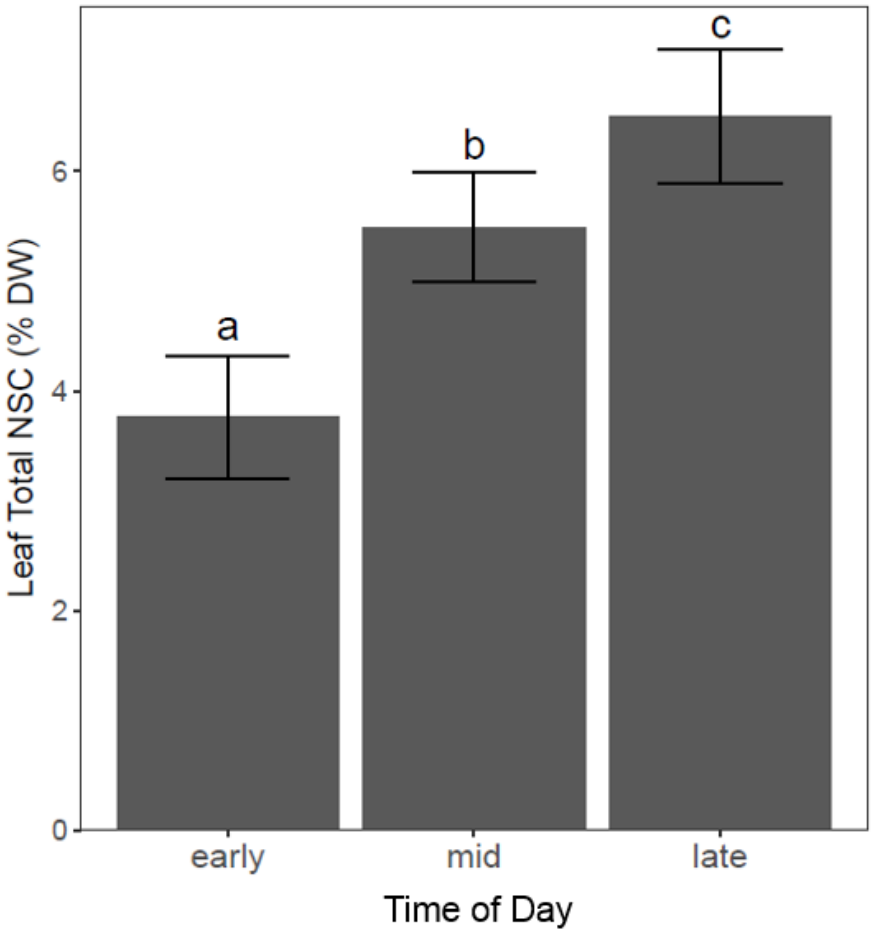

675

676 **Figure S1:** Leaf total NSCs increase over the course of the day. Samples were collected in the
677 morning (early), at mid-day (mid), and before sun-down (late) at all sites in March (n = 22).
678 Error bars are standard errors. Letters indicate significant differences in square root transformed
679 NSC.

680

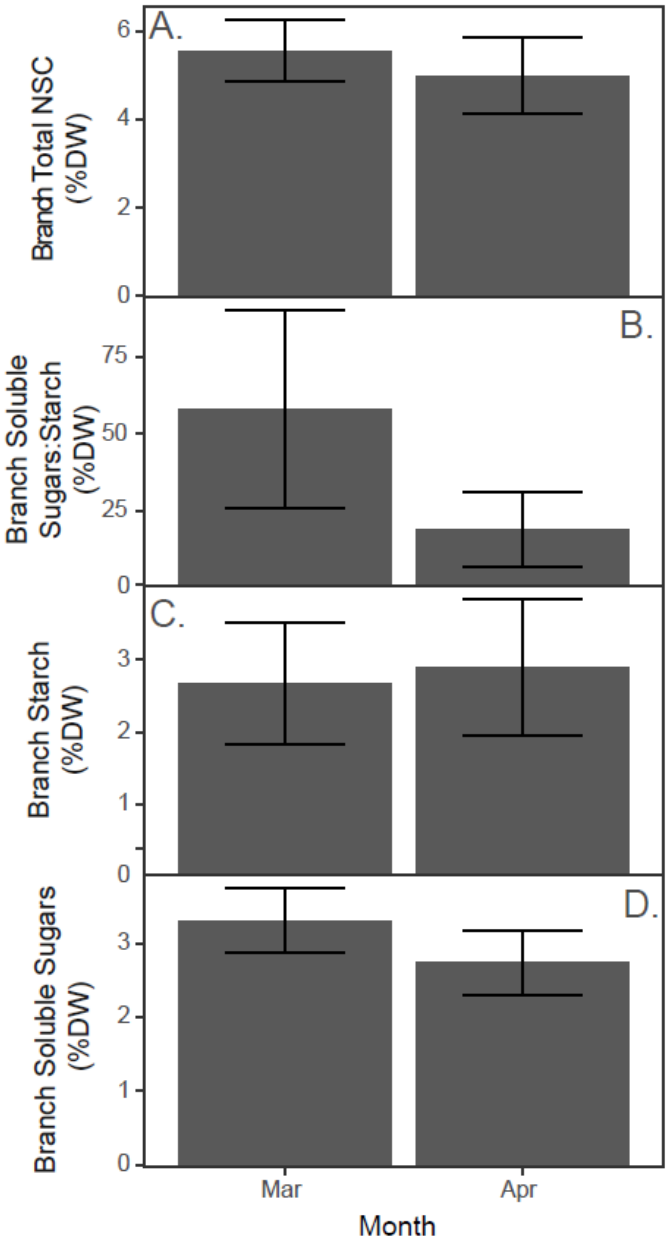

681

682 **Figure S2:** Branch NSCs don't change throughout the drought, though ratio of branch soluble

683 sugars to starch (b) trends lower as drought progresses ($p = 0.16$). Data are from the SLZ site (n

684 $= 18$). Error bars are standard errors.

685

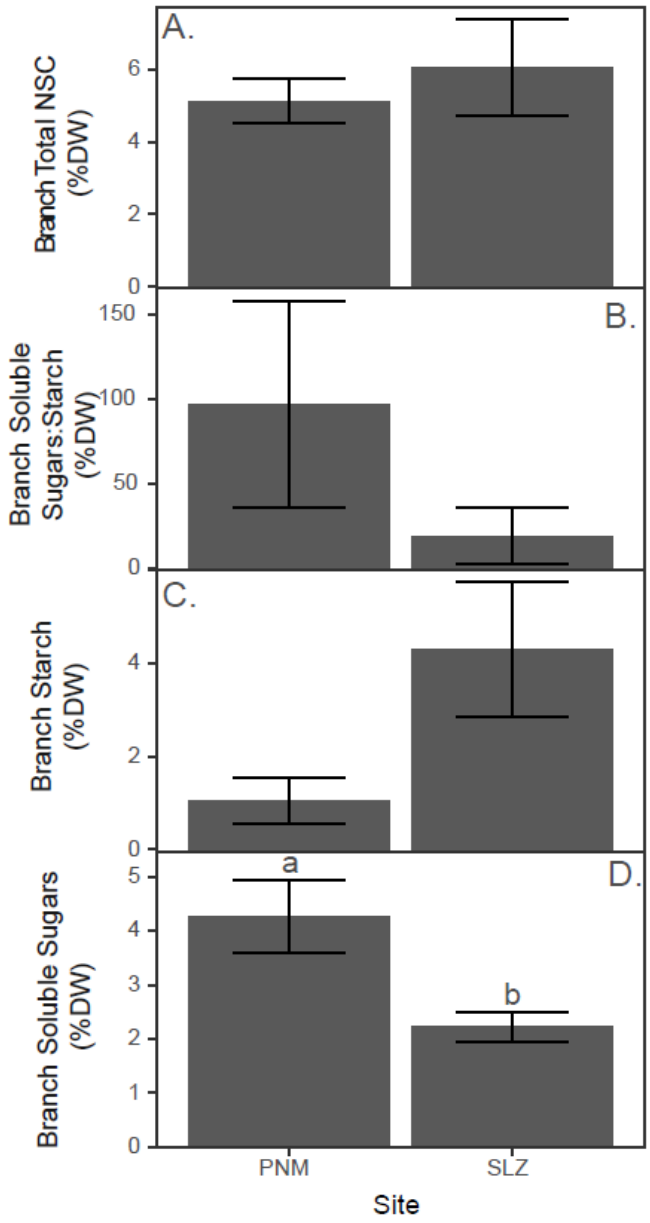

686

687 **Figure S3:** Branch total NSCs (a) don't differ across sites, but ratio of branch soluble sugars to

688 starch (b) trends higher at the drier site (PNM; $p = 0.09$) due to decreasing starch (c; $p = 0.16$)

689 and increased soluble sugars (d; $p = 0.01$). Data are from March (PNM $n = 10$; SLZ $n = 9$). Error

690 bars are standard errors. Letters indicate significant differences ($p \leq 0.05$) in square-root

691 transformed NSC for soluble sugars.

692

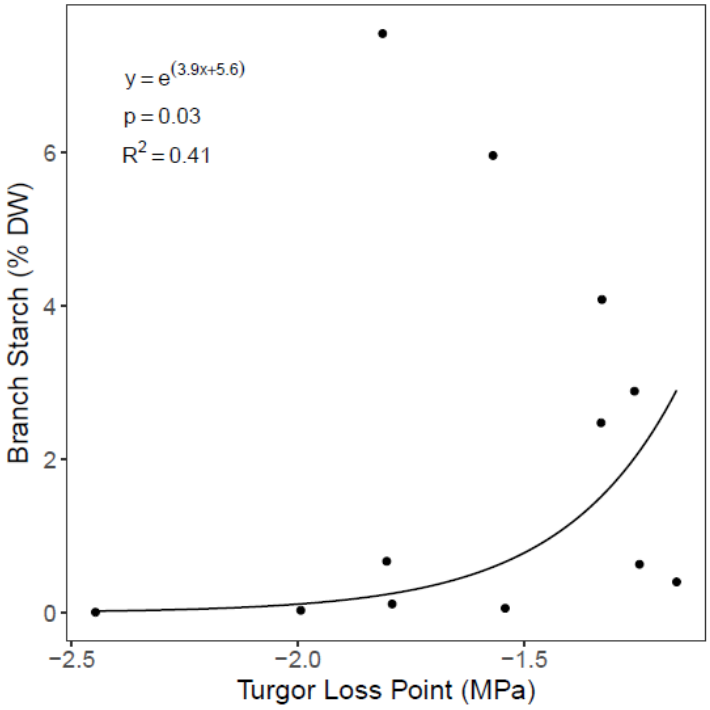

693

694 **Figure S4:** Branch starch increases exponentially with turgor loss point. Each point represents

695 one species.

696

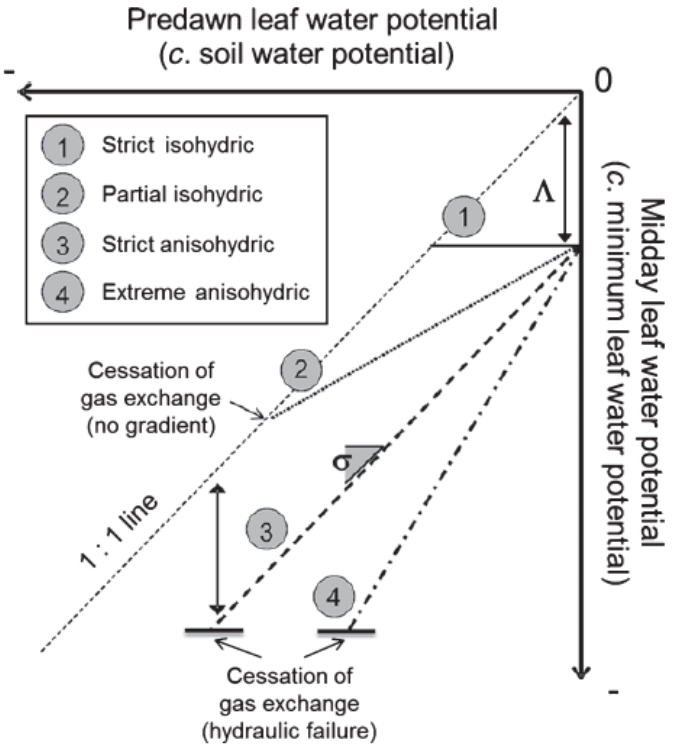

Figure S5: Relationship between predawn (Ψ_{PD}) and midday (Ψ_{MD}) leaf water potentials according to Martinez-Vilalta et al. 2014, Fig. 1. Four different behaviors are depicted, all sharing the same intercept (Λ) but different slopes (σ): strict isohydric ($\sigma = 0$), partial isohydric ($0 < \sigma < 1$), strict anisohydric ($\sigma = 1$) and extreme anisohydric ($\sigma > 1$). The point of cessation of gas exchange is also represented: for isohydric behaviors; it occurs when $\Psi_{PD} = \Psi_{MD}$; for anisohydric relationships, it occurs when Ψ_{MD} reaches the water potential inducing complete loss of plant hydraulic conductance. The 1:1 line is also depicted.

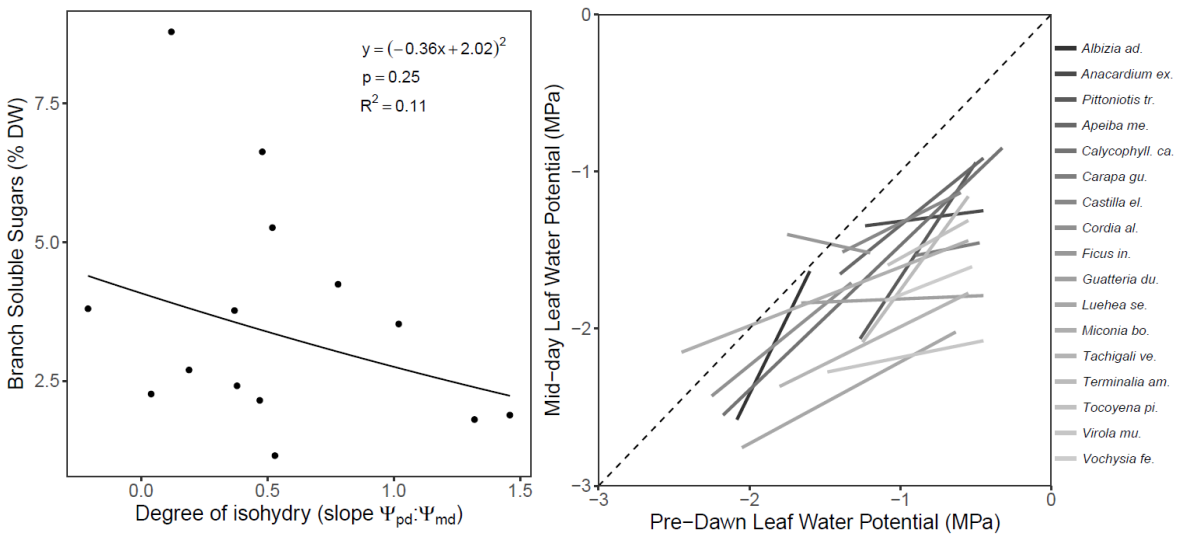

Figure S6: Branch soluble sugars are not related to drought response strategy. Degree of isohydry (a) is defined by the slope of pre-dawn vs. mid-day leaf water potential (b), per Martinez-Villalta et al. (2014) where strict isohydry: slope = 0; partial isohydry 0 < slope < 1; strict anisohydry: slope = 1; extreme anisohydry: slope > 1. Each point represents one species. Species for which range in pre-dawn water potential was less than 0.5MPa (Table S2) were excluded.

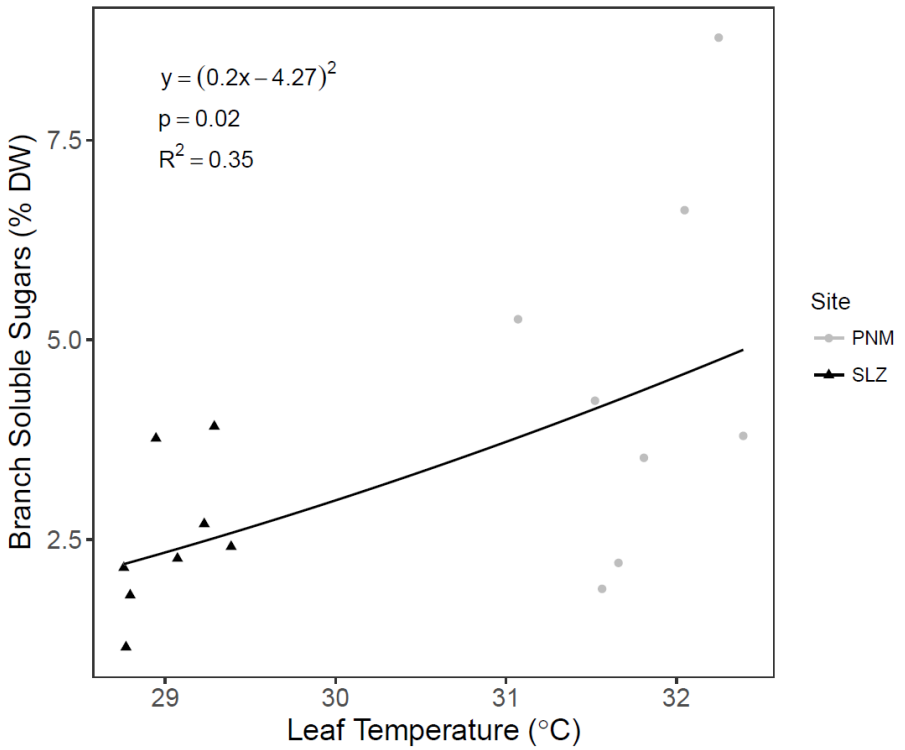

Figure S7: Leaf temperature is consistently higher at the driest site (PNM) compared to the wettest site (SLZ), which may explain the site differences in branch soluble sugars (PNM>SLZ)

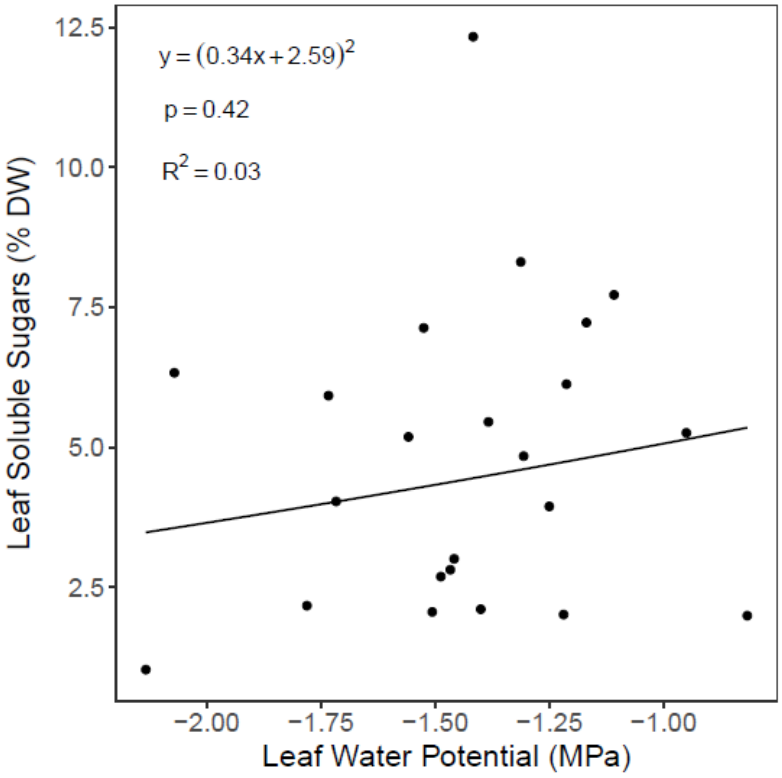

Figure S8: Leaf water potential doesn't explain variation in leaf soluble sugars. NSC data are from the late time point. Each point represents one species.

Table S1: Traits tested for correlation with NSCs. Only significant correlations are shown (see Figure S9).

Trait	Units	Description	Methods detail
T_{leaf}	°C	Sample specific leaf temperature measured with LiCor-6400XT	
A	μmol CO_2 m^{-2} s^{-1}	Sample specific photosynthetic assimilation measured with LiCor-6400XT	
C_i	μmol CO_2 mol^{-1}	Sample specific intercellular CO_2 concentration measured with LiCor-6400XT	
g_s	mol H_2O m^{-2} s^{-1}	Sample specific stomatal conductance measured with LiCor-6400XT	
E	mol m^{-2} s^{-1}	Sample specific transpiration measured with LiCor-6400XT	
Ψ_l	MPa	Sample specific leaf water potential	
LMA_{samp}	g m^{-2}	Sample specific leaf mass per area	
$\Delta\Psi$	MPa	Species specific difference between midday and predawn leaf water potential (from campaigns).	
Ψ_{PD}:Ψ_{MD}	unitless	Slope of relationship between midday and predawn leaf water potential (from campaigns). Metric of isohydry.	See Martinez-Villalta et al. 2014
V_{cmax}	μmol CO_2 m^{-2} s^{-1}	Maximum carboxylation rate extracted from A-C_i curves measured monthly during campaigns	
J_{max}	μmol CO_2 m^{-2} s^{-1}	Maximum electron transport rate extracted from A-C_i curves measured monthly during campaigns	
P_{50}	MPa	Target tree stem water potential at 50% loss of hydraulic conductivity	Stem P_{50} value. Stem water potential at 50% loss of hydraulic conductivity (MPa). Calculated by plotting native stem-area specific hydraulic conductivity as a function of stem water potential and fitting a Weibull curve through the 90% percentile of with quantile regression.
K_{smax}	Kg s^{-1} MPa^{-1} m^{-1}	Target tree maximum stem-area-specific hydraulic conductivity (stem area includes bark and pith)	Maximum stem-area-specific hydraulic conductivity (stem area includes bark and pith). The intercept of the equation described for P_{50} above. Kg s^{-1} MPa^{-1} m^{-1}.
Ψ_{TLP}	MPa	Target tree leaf turgor loss point	Mean leaf turgor loss point (MPa). Calculated from 2-6 pressure volume curves per species. The pressure volume curves were produced with a leaf discs in a psychrometer rather than a whole leaf in a pressure chamber.

Ψ_{bmin}	MPa	Target tree minimum branch water potential measured in the field	Minimum branch water potential measured in the field. (MPa) measured with a pressure chamber at midday on leaves that were bagged and insulated since predawn.
Ψ_{bmax}	MPa	Target tree maximum branch water potential measured in the field	Maximum branch water potential measured in the field. (MPa) with a pressure chamber on leaves that were bagged and insulated at predawn at least 1 h before measurement.
LMA_{sp}	g m^{-2}	Target tree leaf mass per area	
$A_l:A_x$	m^2 m^{-2}	Target tree leaf area per xylem area	
WD_b	g cm^{-3}	Target tree bark density	
WD_{ws}	g cm^{-3}	Target tree whole stem density	
WD_x	g cm^{-3}	Target tree xylem density	

723

Table S2: Study species by site and drought sensitivity metrics. Species specific differences between midday and predawn leaf water potential ($\Delta\Psi$) measured during sampling campaigns and their standard deviations (sd $\Delta\Psi$). Coefficients of the relationship between midday and predawn leaf water potential (intercept and slope Ψ_{PD}:Ψ_{MD}) measured during sampling campaigns. Slope Ψ_{PD}:Ψ_{MD} provides a metric of isohydry (Martinez-Villalta et al. 2014). Species for which the range in measured predawn leaf water potentials ($\Delta\Psi_{PD}$) was less than 0.5 MPa were excluded.

Site	Species	$\Delta\Psi$	sd $\Delta\Psi$	intercept Ψ_{PD}:Ψ_{MD}	slope Ψ_{PD}:Ψ_{MD}	$\Delta\Psi_{PD}$
PNM	*Albizia adinocephala*	0.24	0.31	1.49	1.96	0.48
	Anacardium excelsum	0.50	0.31	-1.19	0.12	0.78
	Pittoniotis trichantha	0.66	0.22	-0.21	1.46	0.77
	Calycophyllum candidissimum	1.09	0.75	-1.05	1.02	1.85
	Castilla elastica	0.30	0.21	-0.85	0.48	0.88
	Cordia alliodora	0.28	0.19	-0.68	0.78	0.93
	Ficus insipida	0.08	0.37	-1.77	-0.21	0.55
	Luehea seemannii	1.02	0.33	-1.69	0.52	1.42
	Pseudobombax septenatum	0.26	NA	-0.89	NA	0
BCI	*Alseis blackiana*	0.61	NA	-1.86	NA	0
	Gustavia superba	0.50	NA	-1.62	NA	0
	Inga pezizifera	0.90	NA	-1.82	NA	0
	Miconia argentea	1.37	NA	-1.93	NA	0
	Simarouba amara	0.75	NA	-1.45	NA	0
SLZ	*Apeiba membranacea*	0.34	0.11	-0.57	0.78	0.95
	Carapa guianensis	0.77	0.31	-1.36	0.19	0.43
	Guatteria dumetorum	0.70	0.61	-1.77	0.04	1.21
	Miconia borealis	0.23	0.50	-1.23	0.37	1.90
	Tachigali versicolor	0.87	0.37	-1.51	0.47	1.25
	Terminalia amazonia	0.74	0.13	-0.43	1.32	0.70
	Tocoyena pittieri	0.61	0.51	-1.02	0.53	0.53
	Virola multiflora	1.29	0.39	-1.99	0.19	1.03
	Vochysia ferruginea	0.86	0.16	-1.41	0.38	0.58

Table S3. Target tree attributes by site.

Site	Species	Phenology	Height (m)	DBH (mm)
PNM	*Albizia adinocephala*	evergreen	29.4	295
	Anacardium excelsum	evergreen	39	1319
	Pittoniotis trichantha	brevideciduous	19	210
	Calycophyllum candidissimum	evergreen	20.1	395
	Castilla elastica	facultative deciduous	23.5	380
	Cordia alliodora	wet season deciduous	22	283
	Ficus insipida	evergreen	31.2	954
	Luehea seemannii	evergreen	26	632
	Pseudobombax septenatum	obligate deciduous	34	1234
BCI	*Alseis blackiana*	brevideciduous	19.1	275
	Gustavia superba	evergreen	15.3	241
	Inga pezizifera	evergreen	25.3	340
	Miconia argentea	evergreen	17.7	239
	Simarouba amara	evergreen	21.7	374
SLZ	*Apeiba membranacea*	brevideciduous	29	805
	Carapa guianensis	evergreen	33.9	620
	Guatteria dumetorum	evergreen	35	590
	Miconia borealis	evergreen	24.8	340
	Tachigali versicolor	evergreen	30.4	574
	Terminalia amazonia	evergreen	27	529
	Tocoyena pittieri	evergreen	26.6	533
	Virola multiflora	evergreen	22.7	351
	Vochysia ferruginea	evergreen	29.4	580

Table S4. NSC sample collection. Text indicates a sample was collected at a given site and date. Green indicates leaf, brown indicates branch. Leaf samples were collected at early, mid-day, or late diurnal time points.

	PNM			BCI			SLZ		
Feb	early		late				early	mid	late
Mar	early	mid	late	early	mid	late	early	mid	late
	branch						branch		
Apr	early						early	mid	late
							branch		
May	early		late				early		late

Table S5. Summary of linear mixed models of leaf NSCs by site (PNM, BCI, SLZ) and time of day (early, mid, late) for each sugar. The response variable is transformed leaf NSC data from March. Significant fixed effects at $p < 0.05$ are bolded.

NSC	Fixed Effects	Random	Correlation	numDF	denDF	F-value	p-value
sqrt(Total NSC)	Intercept	yes	no	1	82	223.03	**<.0001**
	Site			2	19	0.7142	0.5023
	Timeofday			2	82	27.644	**<.0001**
log(Starch)	Intercept	yes	no	1	38	11.484	**0.0016**
	Site			2	16	0.1137	0.8932
	Timeofday			2	38	7.7839	**0.0015**
sqrt (Soluble Sugars)	Intercept	yes	no	1	80	171.27	**<.0001**
	Site			2	19	0.4172	0.6648
	Timeofday			2	80	17.784	**<.0001**
log (SS:Starch)	Intercept	yes	no	1	36	39.985	**<.0001**
	Site			2	16	0.1340	0.8756
	Timeofday			2	36	1.3621	0.2690

Note: Full model: lme(NSC ~ Site + Timeofday, random=~1|Species/Sample_ID, na.action=na.exclude, method="REML", correlation = corAR1(form=~Timeofday|Species/Sample_ID))

Table S6: Parameter estimates from linear mixed models of leaf NSCs by site and time of day for each sugar. The response variable is transformed leaf NSC data from March. Letters indicate significant differences at $p < 0.05$.

	early	mid	late
sqrt(leaf TNSC)	**1.77 a**	**2.22 b**	**2.43 c**
log(leaf Starch)	**-1.97 a**	**-0.83 b**	**-0.53 b**
sqrt(leaf SS)	**1.70 a**	**2.08 b**	**2.19 b**
log(leaf SS:Starch)	2.47	2.2	1.85

Table S7. Summary of linear mixed models of NSCs by site (PNM, BCI, SLZ) and month (Feb, Mar, Apr, May) for each tissue and sugar. The response variable is transformed NSC data. For leaves, data are from the late time point. Significant fixed effects at $p < 0.05$ are bolded.

NSC	Fixed Effects	Random	Correlation	numDF	denDF	F-value	p-value
sqrt(leaf TNSC)	Intercept	Yes	no	1	79	575.38	**<.0001**
	Site			2	20	0.0979	0.9072
	Month			3	79	1.1843	0.3211
log(leaf Starch)	Intercept	yes	no	1	79	5.9238	**0.0172**
	Site			2	20	0.3537	0.7064
	Month			3	79	8.4823	**0.0001**
sqrt(leaf SS)	Intercept	yes	no	1	79	245.03	**<.0001**
	Site			2	20	0.0150	0.9851
	Month			3	79	3.3796	**0.0223**
log(leaf SS:Starch)	Intercept	yes	no	1	62	22.957	**<.0001**
	Site			2	20	0.0653	0.9370
	Month			3	62	10.909	**<.0001**
sqrt(branch TNSC)	Intercept	no	yes	1	25	265.31	**<.0001**
	Site			1	-	0.0025	0.9603
	Month			1	-	1.1196	0.3001
log(branch Starch)	Intercept	no	yes	1	20	0.7137	0.4082
	Site			1	-	1.7567	0.2000
	Month			1	-	1.4835	0.2374
sqrt(branch SS)	Intercept	no	no	1	25	492.62	**<.0001**
	Site			1	-	8.7087	**0.0068**
	Month			1	-	0.4851	0.4925
log(branch SS:Starch)	Intercept	no	yes	1	14	7.4502	**0.0163**
	Site			1	14	2.7115	0.1219
	Month			1	6	2.2392	0.1852

Note: Full model: lme(NSC ~ Site + Month, random=~1|Species/Sample_ID, na.action=na.exclude, method="REML", correlation = corAR1(form=~Month|Species/Sample_ID))

Table S8. Summary of linear mixed models of branch NSCs from the SLZ site by month (Mar, Apr) for each sugar. The response variable is transformed branch NSC data. Significant fixed effects at $p < 0.05$ are bolded.

NSC	Fixed Effects	Random	Correlation	numDF	denDF	F-value	p-value
sqrt(TNSC)	Intercept	no	yes	1	16	95.283	**<.0001**
	Month			1	-	1.0094	0.33
log(Starch)	Intercept	no	yes	1	13	0.1101	0.7453
	Month			1	-	1.4870	0.2443
sqrt(SS)	Intercept	no	no	1	16	348.91	**<.0001**
	Month			1	-	0.6586	0.429
log(SS:Starch)	Intercept	no	yes	1	13	0.6948	0.4196
	Month			1	-	2.2480	0.1577

Note: Full model: lme(NSC ~ Month, random=~1|Species/Sample_ID, na.action=na.exclude, method="REML", correlation = corAR1(form=~Month|Species/Sample_ID))

Table S9. Summary of linear mixed models of branch NSCs from March by site (PNM, SLZ) for each sugar. The response variable is transformed branch NSC data. Significant fixed effects at p < 0.05 are bolded.

NSC	Fixed Effects	Random	numDF	denDF	F-value	p-value
sqrt(TNSC)	Intercept	no	1	17	238.97	**<.0001**
	Site		1	-	0.1389	0.714
log(Starch)	Intercept	no	1	14	0.4479	0.5142
	Site		1	-	2.2224	0.1582
sqrt(SS)	Intercept	no	1	17	364.15	**<.0001**
	Site		1	-	8.6057	**0.0093**
log(SS:Starch)	Intercept	no	1	14	5.9514	**0.0286**
	Site		1	-	3.3879	0.0870

Note: Full model: lme(NSC ~ Site, random=~1|Species/Sample_ID, na.action=na.exclude, method="REML")

Table S10: Parameter estimates from linear mixed models of NSCs by month for each tissue and sugar. The response variable is transformed NSC data. For leaves, data are from the late time point. Letters indicate significant differences at $p < 0.05$.

	Feb	**Mar**	**Apr**	**May**
sqrt(leaf TNSC)	2.38	2.44	2.43	2.61
log(leaf Starch)	**-0.27 a**	-0.58 a	0.18ab	**0.67b**
sqrt(leaf SS)	2.08 ab	**2.21 a**	1.94 ab	**1.91 b**
log(leaf SS:Starch)	**1.75 ab**	**2.02a**	**1.05bc**	**0.5c**
sqrt(branch TNSC)	-	2.28	2.11	-
log(branch Starch)	-	-0.36	0.02	-
sqrt(branch SS)	-	1.76	1.61	-
log(branch SS:Starch)	-	1.43	2.29	-

Table S11: Parameter estimates from linear mixed models of NSCs by site for each tissue and sugar. The response variable is transformed NSC data. For leaves, data are from the late time point. Letters indicate significant differences at $p < 0.05$.

	PNM	**BCI**	**SLZ**
sqrt(leaf TNSC)	2.51	2.38	2.46
log(leaf Starch)	0.09	-0.27	-0.06
sqrt(leaf SS)	2.08	2.03	2.08
log(leaf SS:Starch)	1.26	1.59	1.42
sqrt(branch TNSC)	2.22	-	2.23
log(branch Starch)	-1.16	-	0.24
sqrt(branch SS)	**2.01 a**	-	**1.54 b**
log(branch SS:Starch)	2.51	-	0.64

Table S12. Summary of linear mixed models of NSCs by species (leaves n = 23; branches n = 18) for each tissue and sugar. The response variable is transformed NSC data. For leaves, data are from the late time point. Significant fixed effects at $p < 0.05$ are bolded.

NSC	Fixed Effects	Random	Correlation	numDF	denDF	F-value	p-value
sqrt(leaf TNSC)	Intercept	no	no	1	109	2892.5	**<.0001**
	Species			22	-	3.9182	**<.0001**
log(leaf Starch)	Intercept	no	no	1	90	0.0037	0.9515
	Species			22	-	2.7070	**0.0005**
sqrt(leaf SS)	Intercept	no	no	1	109	3034.5	**<.0001**
	Species			22	-	10.472	**<.0001**
log(leaf SS:Starch)	Intercept	no	no	1	90	109.49	**<.0001**
	Species			22	-	5.1682	**<.0001**
sqrt(branch TNSC)	Intercept	no	no	1	10	914.55	**<.0001**
	Species			17	-	3.5639	**0.0229**
log(branch Starch)	Intercept	no	no	1	7	2.1559	0.1855
	Species			15	-	11.783	**0.0015**
sqrt(branch SS)	Intercept	no	no	1	10	1041.7	**<.0001**
	Species			17	-	3.6649	**0.0208**
log(branch SS:Starch)	Intercept	no	no	1	7	46.927	**0.0002**
	Species			15	-	10.090	**0.0024**

Note: Full model: lme(NSC ~ Species, random=~1|Site or ~Month|Site/Sample_ID, na.action=na.exclude, method="REML", correlation = corAR1(form=~Month|Site/Sample_ID))

Table S13. Summary of linear mixed models of NSCs by traits for select tissues and sugars. The response variable is transformed NSC data. For leaves, data are from the late time point. Traits with significant relationships (bolded, $p < 0.05$) to NSCs include LMA (leaf mass per area, g dw m^{-2}), Ψ_{TLP} (turgor loss point, MPa), *A* (photosynthetic assimilation, μmol m^{-2} s^{-1}), WD_x (xylem wood density, g cm^{-3} m^{-1}), and T_{leaf} (leaf temperature, °C). Ψ_{PD}:Ψ_{MD} (slope of pre-dawn to mid-day leaf water potential, unitless) was also included as a metric for relative isohydry, however there was no significant relationship to NSCs. Other non-significant relationships are not shown. Traits are species averages.

NSC	Fixed Effects	Random	Correlation	numDF	denDF	F-value	p-value
sqrt(leaf TNSC)	Intercept	no	no	1	21	732.17	**<.0001**
	LMA			1	-	9.2092	**<.0063**
log(branch Starch)	Intercept	no	no	1	10	1.6751	0.2247
	Ψ_{TLP}			1	-	6.8477	**0.0257**
sqrt(branch SS)	Intercept	no	no	1	14	270.14	**<.0001**
	A			1	-	4.5958	**0.0501**
sqrt(branch SS)	Intercept	no	no	1	14	392.97	**<.0001**
	WD_x			1	-	13.052	**0.0028**
sqrt(branch SS)	Intercept	no	no	1	14	315.21	**<.0001**
	T_{leaf}			1	-	7.6984	**0.0149**
sqrt(branch SS)	Intercept	no	no	1	14	235.89	**<.0001**
	Ψ_{PD}:Ψ_{MD}			1	-	2.2380	0.1569

Note: Full model: lme(NSC ~ Trait, random=~1|Species or ~Month|Species, na.action=na.exclude, method="REML", correlation = corAR1(form=~Month|Species))